ELSEVIER

Journal of Organometallic Chemistry 637–639 (2001) 276–283

Journal of Organometallic Chemistry

www.elsevier.com/locate/jorganchem

Synthesis, characterisation, crystal structures and electrochemistry of triosmium nitrite carbonyl clusters containing ferrocenyl phosphines

Emmie Ngai-Man Ho *, Bernard Kwok-Man Hui, Wing-Tak Wong *

Department of Chemistry, The University of Hong Kong, Pokfulam Road, Hong Kong, Hong Kong

Received 2 January 2001; received in revised form 6 March 2001; accepted 10 April 2001

Abstract

The triosmium nitrite carbonyl cluster $[Os_3(\mu\text{-}H)(CO)_{10}(\mu\text{-}\eta^2\text{-}NO_2)]$ (**1**) was allowed to react with 1,1′-bis(diphenylphosphino)ferrocene (dppf) and *N*,*N*-dimethyl-1-[(*S*)-2-(diphenylphosphino)ferrocenyl]ethylamine (ppfa) in the presence of Me_3NO in CH_2Cl_2, and clusters $[Os_3(\mu\text{-}H)(CO)_8(\mu\text{-}\eta^2\text{-}NO_2)(\mu\text{-dppf})]$ (**2**) and $[Os_3(\mu\text{-}H)(CO)_8(\mu\text{-}\eta^2\text{-}NO_2)(\mu\text{-ppfa})]$ (**3**) were afforded in moderate yields. Clusters **2** and **3** were fully characterised by spectroscopic techniques and X-ray crystallography. The nitrite, hydride and the ferrocenyl phosphine ligands are all bridged across the same Os–Os edge. The amine group of the ppfa ligand shows a preference to coordinate with the Os atom with a σ-bonded nitrite O atom. The redox properties of the nitrite complexes were investigated using cyclic voltammetry.

Keywords: Osmium; Cluster; Nitrite; Ferrocene; Electrochemistry

1. Introduction

The synthesis and reactions of triosmium nitrite carbonyl clusters have been a subject of our interest [1–3]. Much of our attention has been focused on the synthesis and properties of nitrite-containing clusters with functionalised phosphine [2] and amine [3] ligands. It is believed that the presence of an electron-withdrawing $\mu\text{-}\eta^2\text{-}NO_2$ group on the cluster framework would have a pronounced effect on the cluster reactivity, which should be revealed through the ligand addition and substitution reactions. Metallocenes, in particular ferrocene, possess properties that have led to their use as ferromagnets [4,5], molecular sensors [6–8], and electrochemical agents [9]. During the last few years, bi- and multi-functional ferrocene derivatives have been used successfully as ligands for homogeneous catalysts [10], and further development of new ligands is an interesting area of research. Among these, ferrocenylphosphines, in particular 1,1′-bis(diphenylphosphino)ferrocene (dppf) and *N*,*N*-dimethyl-1-[(*S*)-2-(diphenylphosphino)ferrocenyl]ethylamine (ppfa), have been extensively employed as chelating agents for transition-metal complexes, and show interesting properties and are also widely utilised in metal carbonyl complexes [11–15]. Ferrocenyl-based chiral ligands have been examined in a number of enantioselective reactions such as hydrogenation, hydrosilylation, cross-coupling reactions, the addition of dialkylzinc to aldehydes, aldol type condensations, amongst others [16,17]. The incorporation of this redox active moiety into the cluster framework is a good candidate for the study of the multiple oxidation states that these compounds exhibit. It is believed that the reaction of the nitrite cluster with asymmetric ferrocenyl phosphine will also be useful to investigate the site selectivity of the substitution of CO onto the cluster, which may give us some insight into the chemistry of the nitrite clusters.

* Corresponding authors. Fax: +86-852-2547-2933.
E-mail address: wtwong@hkucc.hku.hk (W.-T. Wong).

0022-328X/01/$ - see front matter
PII: S0022-328X(01)00918-4

In this paper, we report the facile synthesis of the complexes $[Os_3(\mu\text{-}H)(CO)_8(\mu\text{-}\eta^2\text{-}NO_2)(\mu\text{-dppf})]$ (**2**) and $[Os_3(\mu\text{-}H)(CO)_8(\mu\text{-}\eta^2\text{-}NO_2)(\mu\text{-ppfa})]$ (**3**) by the oxidative decarbonylation of $[Os_3(\mu\text{-}H)(CO)_{10}(\mu\text{-}\eta^2\text{-}NO_2)]$ (**1**) with Me_3NO in the presence of the ferrocenylphosphines, dppf and ppfa. In order to investigate the redox properties of these nitrite carbonyl clusters, the electrochemistry of clusters **1**–**3** and a related cluster anion $[Os_3(CO)_{10}(\mu\text{-}\eta^2\text{-}NO_2)]^-$ [1] were studied.

2. Results and discussion

2.1. Synthesis and characterisation

2.1.1. Reaction of $[Os_3(\mu\text{-}H)(CO)_{10}(\mu\text{-}\eta^2\text{-}NO_2)]$ (1) with dppf

Cluster **1** was treated with dppf and Me_3NO in CH_2Cl_2 at room temperature (r.t.) to give a red cluster $[Os_3(\mu\text{-}H)(CO)_8(\mu\text{-}\eta^2\text{-}NO_2)(\mu\text{-dppf})]$ (**2**) in 46% yield (Scheme 1). A summary of the spectroscopic data is

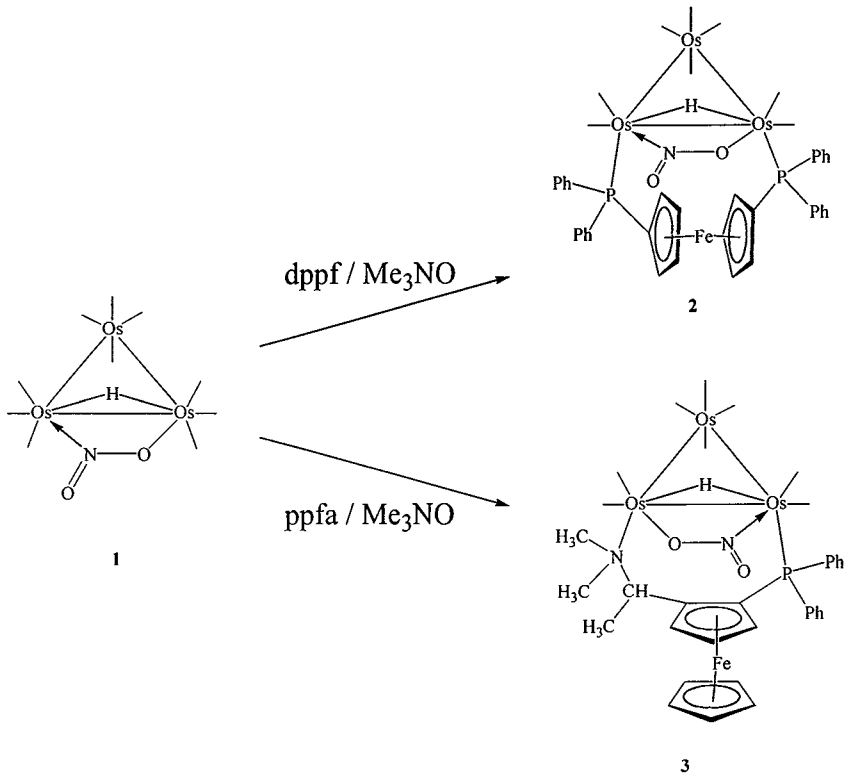

Scheme 1.

Table 1
Spectroscopic data for clusters **1**–**3**

Cluster	IR spectra [a], ν (CO) (cm^{-1})	^{1}H-NMR spectra [b], (δ, J (Hz))	^{31}P-NMR spectra [c], (δ)	Mass spectra [d], (m/z)
2	2080s, 2020vs, 2010vs, 1997s, 1968w 1949w	7.6 (m, 8H, Cp) 7.4 (m, 20H, phenyl) −10.0 (s br, 1H, Os–H	2.1 1.3	1396 (1396)
3	2083s, 2006vs, 1966w, 1940w, 1923w	8.3 (m, 3H, Cp) 7.6 (s, 5H, Cp) 7.4 (m, 10H, phenyl) 3.5 (s br, 6H, NCH_3) 1.1 (s, 1H, CH) 0.8 (s, 3H, CH_3) −10.4 (s br, 1H, Os–H)	17.5	1283 (1283)

[a] In CH_2Cl_2 unless otherwise stated.
[b] In CD_2Cl_2.
[c] In $CDCl_3$, with ^{1}H decoupled.
[d] Calculated values in parentheses.

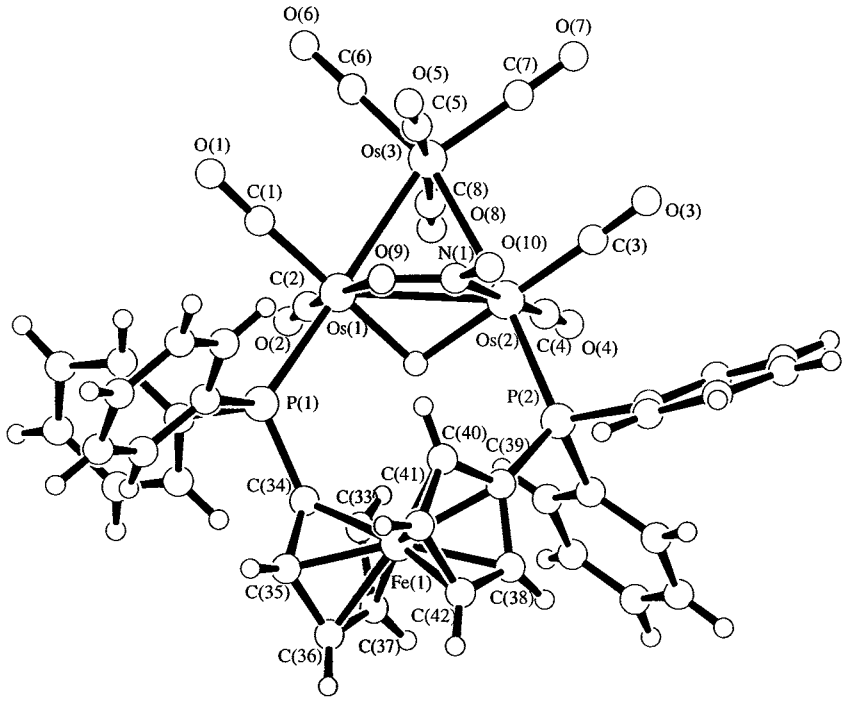

Fig. 1. The molecular structure of $[Os_3(\mu\text{-}H)(CO)_8(\mu\text{-}\eta^2\text{-}NO_2)(\mu\text{-dppf})]$ (**2**) with the atom-numbering scheme.

given in Table 1, in which all spectroscopic data are found to be fully consistent with the solid state structure of **2**. Eight terminal carbonyls are associated with the metal core. A hydride ligand is bridged across one of the Os–Os edges, with the resonance signal observed at δ −10.0 in its ^{1}H-NMR spectrum. Solid-state IR spectroscopy revealed the stretching frequencies of the coordinated NO_2 group at 1478 and 1122 cm^{-1}. This is comparable to the values observed in the parent cluster **1** [1]. Single crystals were obtained from a saturated CH_2Cl_2 solution by slow evaporation. The molecular structure of **2** was established by X-ray analysis. Two molecules of CH_2Cl_2, as solvent of crystallisation, were revealed in the asymmetric unit. The geometry of cluster **2** is presented in Fig. 1 and the pertinent bond parameters are summarised in Table 2.

The metal framework is found to be an irregular triangle with the Os(1)–Os(2) being the longest edge [2.9314(8) Å]. The hydride, the nitrite ligand and the dppf are all bridged across this long edge. The bridging nitrite moiety is bonded to the edge via bonds [Os(2)–N(1) 2.082(9) and Os(1)–O(9) 2.158(8) Å]. The N–O bond distances in the μ-η^2-NO_2 moiety are O(9)–N(1) 1.28(1) Å and O(10)–N(1) 1.23(1) Å. The dihedral angle defined by the nitrite ligand and the metal framework is 78.8°, which is significantly smaller than that in the starting cluster **1** (102.3°) [1]. This may be attributed to the steric interaction with the bulky dppf substituent on cluster **2**. The organic dppf moiety is bridged across Os(1) and Os(2) and displays two separated signals in its ^{31}P-NMR spectrum. The dppf ligand is terminally coordinated to the cluster via P(1) [Os(1)–P(1) 2.381(3) Å] and P(2) [Os(2)–P(2) 2.357(3) Å] and are arranged equatorially so that steric interaction between the phenyl rings and adjacent CO ligands

Table 2
Selected bond lengths (Å) and bond angles (°) for clusters **2** and **3**

	2	**3**
Os(1)–Os(2)	2.9314(8)	2.908(2)
Os(1)–Os(3)	2.8732(7)	2.831(2)
Os(2)–Os(3)	2.8676(7)	2.849(1)
Os(1)–P(1)	2.381(3)	–
Os(1)–O(9)	2.158(8)	2.14(2)
Os(1)–N(2)	–	2.34(3)
Os(2)–P(1)	–	2.359(7)
Os(2)–P(2)	2.357(3)	–
Os(2)–N(1)	2.082(9)	2.07(2)
O(9)–N(1)	1.28(1)	1.31(3)
O(10)–N(1)	1.23(1)	1.25(5)
Os(2)–Os(1)–Os(3)	59.20(2)	59.51(4)
Os(1)–Os(2)–Os(3)	59.39(2)	58.90(4)
Os(1)–Os(3)–Os(2)	61.41(2)	61.59(4)
Os(2)–Os(1)–P(1)	121.08(8)	–
Os(2)–Os(1)–O(9)	67.2(2)	65.7(7)
Os(2)–Os(1)–N(2)	–	111.1(7)
Os(1)–Os(2)–P(1)	–	107.1(2)
Os(1)–Os(2)–P(2)	115.45(7)	–
Os(1)–Os(2)–N(1)	66.7(3)	69.5(7)
Os(1)–O(9)–N(1)	109.3(6)	113(1)
Os(2)–N(1)–O(9)	116.5(7)	113(1)
Os(2)–N(1)–O(10)	127.4(7)	141(2)
O(9)–N(1)–O(10)	116.0(9)	107(2)

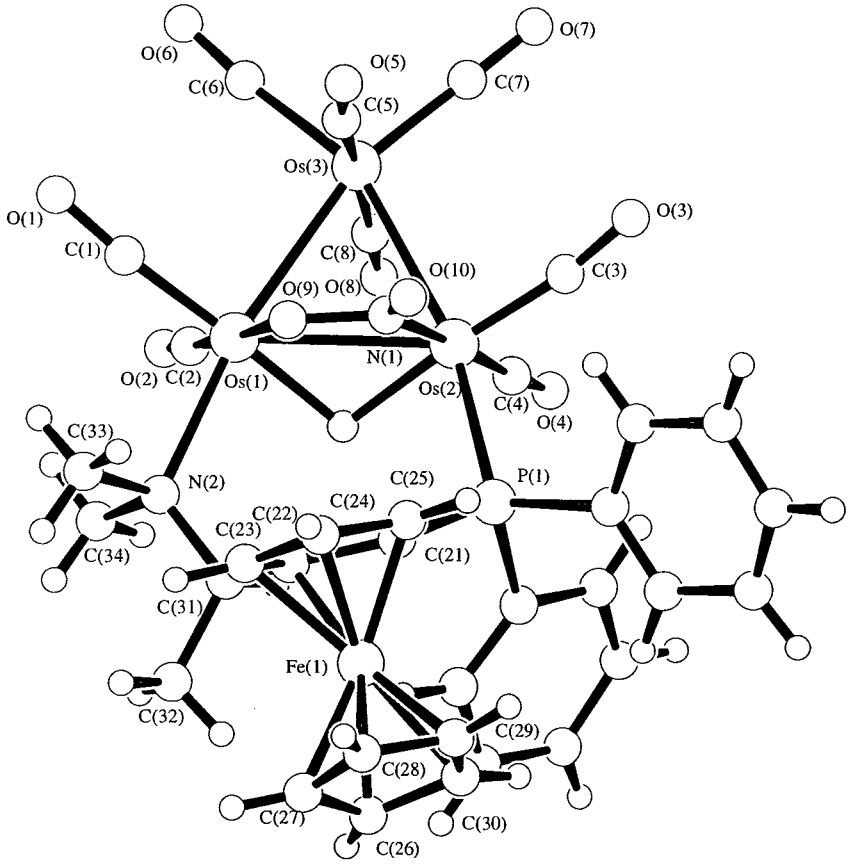

Fig. 2. The molecular structure of $[Os_3(\mu\text{-}H)(CO)_8(\mu\text{-}\eta^2\text{-}NO_2)(\mu\text{-}ppfa)]$ (**3**) with the atom numbering scheme.

is minimised. The two cyclopentadienyl rings are arranged in an eclipsed conformation, as confirmed by X-ray structural determination. They are almost parallel with each other, have a tilted angle of 4.7°, and distances of 1.652 and 1.650 Å from their centroids to the iron centre. The average Fe–C (cyclopentadienyl) distance and C–C bond length in the ferrocene moiety are 2.05 and 1.42 Å, respectively, which is comparable to other compounds containing dppf. There is no significant interaction between the Fe atom in the dppf moiety and the osmium cluster core.

2.1.2. Reactions of $[Os_3(\mu\text{-}H)(CO)_{10}(\mu\text{-}\eta^2\text{-}NO_2)]$ (1) with ppfa

The treatment of cluster **1** with ppfa in the presence of Me_3NO in CH_2Cl_2 at 40 °C resulted in a colour change from yellow to dark red. The reaction was monitored by IR and TLC until the complete consumption of **1**. The red solution was concentrated under reduced pressure and the residue separated by TLC to give one intensive red band. It was characterised as $[Os_3(\mu\text{-}H)(CO)_8(\mu\text{-}\eta^2\text{-}NO_2)(\mu\text{-}ppfa)]$ (**3**) in 40% yield (Scheme 1). The spectroscopic data are given in Table 1. Single crystals of **3** suitable for X-ray analysis were obtained from a $CHCl_3$–*n*-hexane solution by slow evaporation. The solid state structure of cluster **3** was established by X-ray crystallography. A perspective view of **3** is shown in Fig. 2. Selected intramolecular bond distances and angles are listed in Table 2. The IR spectrum indicates that only terminal carbonyls are bonded to the metal core. The ^{1}H-NMR spectrum of **3** exhibits a hydride signal at δ −10.4, while a signal at δ 3.5 for the methyl protons of the amine group is observed. The ^{31}P-NMR spectrum exhibits a phosphorus signal at δ 17.5. The stretching frequencies of the coordinated NO_2 group are found at 1481 and 1129 cm^{-1}. The positive fast atom bombardment (FAB) mass spectrum shows a molecular ion peak at m/z 1284, together with daughter ions due to the sequential losses of eight carbonyls.

Cluster **3** crystallises in the orthorhombic space group $P2_12_12_1$ with four molecules in the unit cell. The $Os_3(NO_2)$ core is similar to that of cluster **2**. The three osmium atoms in cluster **3** define an irregular triangle. The Os(1)–Os(2) edge is bridged by a hydride, a bridging nitrite and the ppfa ligands. The Os–Os distances observed in **3** are significantly shorter than the corresponding one in **2**. This is believed to be the result of different electronic effects of the N-donor in **3** and P-donor in **2**. A similar difference has been observed for $[Os_3(\mu\text{-}H)(CO)_{10-x}(\mu\text{-}\eta^2\text{-}NO_2)(PPh_3)_x]$, $x = 1, 2$ in which the disubstituted product gives longer Os–Os distances [2]. The nitrite ligand is coordinated to the osmium atoms through N(1) and O(9) atoms, and is

attached to Os(2) through a dative bond from N(1) [Os(2)–N(1) 2.07(2) Å] and bonded to Os(1) with a σ bond from O(9) [Os(1)–O(9) 2.14(2) Å]. The N–O bond lengths in the nitrite moiety are [O(9)–N(1) 1.31(3) and O(10)–N(1) 1.25(5) Å], and O(9)–N(1)–O(10) is equal to 107(2)°. The dihedral angle between the planes defined by the triosmium metal core and the nitrite moiety is 78.3°. The ppfa ligand bridges across the Os(1) and Os(2) edge with N(2) [Os(1)–N(2) 2.34(3) Å] and P(1) [Os(2)–P(1) 2.359(7) Å] atoms. The general structural features of the ferrocene unit of **3** is very similar to that of **2**: the average Fe–C (cyclopentadienyl) bond length is 2.00 Å, and the average C–C bond distance is 1.39 Å. The eclipsed nature of the rings is established by structural analysis and they are found to have distances of 1.633 and 1.587 Å from their centroids to the iron atom. The ferrocenyl cyclopentadienyl (Cp) rings are not parallel with respect to each other (dihedral angle, 12.3°). The asymmetrically bridging nitrite ligand leads to differences in strength of back π bonding to their adjacent carbonyl groups, which in turn, affects the ease of substitution of these CO groups. We have isolated just one isomer with the phosphine P atom bonded to Os(2) and the nitrite N(2) atom coordinated, from the reaction between cluster **1** and ppfa. The site selectivity observed in this case may be due to the combined effect of difference in donor capacity between P and N and the electronic imbalance between two osmium centres. The more electron-accepting phosphine fragment appears to prefer Os(2), which has a dative bond from N(1) and is more electron rich, whilst the amine nitrogen substituted the carbonyl on Os(1) to where O(9) σ-bonded. Although these results are consistent with the previous studies with functionalised phosphine and amine ligands [2,3], we could not rule out the possibility of formation of the other isomers in minute quantity.

Table 3
Electrochemical data [a] for compounds **1**–**3**

Cluster	Oxidation		Reduction	
	E_{pa2} (V) [b]	E_{pa1} (V) [b]	E_{pc1} (V) [b]	E_{pc2} (V) [b]
$[Os_3(CO)_{10}$-$(\mu\text{-}\eta^2\text{-}NO_2)]^-$	0.96	0.08	−2.23	−2.73
1	–	0.78	−1.73	−2.17
2	–	(0.61) [c]	−2.03	–
3	–	(0.33) [c]	−2.15	–

[a] $\sim 10^{-3}$ M cluster in 0.1 M TBAHFP in acetonitrile at 298 K, the working electrode was a glassy carbon electrode, the auxiliary electrode and the reference electrode were a platinum wire and $Ag \mid AgNO_3$, respectively. Scan rate was 100 mV s^{-1}. The potentials are referenced to the $Ag \mid AgNO_3$ (0 V) under the same conditions, calibrated with ferrocene.

[b] E_{pa} and E_{pc} are the anodic and cathodic potentials, respectively.

[c] Values in parentheses is $E_{1/2}$, half-wave potential values.

2.2. Electrochemistry

Incorporation of the redox-active ferrocenyl groups in the cluster framework may lead to interesting electrochemical properties as these groups are well known to be excellent electron donors. Electronic and/or electrostatic communications between redox-active centres have been observed in some ferrocene-containing metal complexes and cluster compounds [18]. The electrochemical behaviour of clusters **1**–**3** has been examined in CH_2Cl_2 using cyclic voltammetry, with *n*-tetrabutylammonium hexafluorophosphate (TBAHFP) as a supporting electrolyte. The redox potential values obtained are summarised in Table 3.

Cluster anion $[Os_3(CO)_{10}(\mu\text{-}\eta^2\text{-}NO_2)]^-$ displays two irreversible reductions at −2.23 and −2.73 V at a scan rate of 100 mV s^{-1}. It is believed that the metal core of the cluster is reduced to give the 49e$^-$ species $[Os_3(CO)_{10}(NO_2)]^{2-}$, and then further reduced to give the 50e$^-$ species $[Os_3(CO)_{10}(NO_2)]^{3-}$, both being very unstable. The first oxidation at 0.08 V corresponds to the oxidation of the triosmium core to give the 47e$^-$ species $[Os_3(CO)_{10}(NO_2)]$ and the second one is assigned to the further oxidation of these 47e$^-$ species to give the 46e$^-$ species $[Os_3(CO)_{10}(NO_2)]^+$. The protonated derivative of $[Os_3(CO)_{10}(\mu\text{-}\eta^2\text{-}NO_2)]^-$, cluster **1**, exhibits two irreversible reductions at −1.73 and −2.17 V and these potentials are significantly increased as compared to the corresponding potentials of $[Os_3(CO)_{10}(\mu\text{-}\eta^2\text{-}NO_2)]^-$ (−2.23 and −2.73 V). These redox couples are metal-oriented, as there are great differences between the anionic metal complex and the neutral metal complex. The $Os_3(NO_2)$ core of cluster **1** is electron deficient as compared with that of the anionic cluster $[Os_3(CO)_{10}(\mu\text{-}\eta^2\text{-}NO_2)]^-$. As a result, the reduction process in $[Os_3(CO)_{10}(\mu\text{-}\eta^2\text{-}NO_2)]^-$ is less favourable and the reduction potentials are shifted to a more negative region. The irreversible oxidation of **1** is assigned to the oxidation of the triosmium core to form the 47e$^-$ species $[Os_3(H)(CO)_{10}(NO_2)]^+$. Cluster **2** contains an electroactive dppf ligand and the intramolecular redox reactivity is useful for investigating the electrochemical properties of the triosmium nitrite cluster. The cyclic voltammogram of **2** exhibits a quasi-reversible oxidation wave at $E_{1/2} = 0.61$ V versus $Ag \mid AgNO_3$ in acetonitrile. It is likely that this anodic wave is dppf-based in nature, as it occurs at a similar potential as the free dppf ligand ($E_{1/2} = 0.55$ V). In this context, it is evident that the ferrocene–ferrocenium couple in **2** is subjected to minor electronic influence imposed by the triosmium nitrite cluster unit. In addition, cluster **2** displays an irreversible reduction at −2.03 V that is assigned to the reduction of the triosmium core, to form the 49e$^-$ species $[Os_3(H)(CO)_8(NO_2)(dppf)]^-$, which exhibits a cathodic shift of 0.30 V. Cluster **3** also contains an electrochem-

ically active ligand, ppfa. The redox property of **3** is very similar to that of **2**. In cluster **3**, the ppfa moiety gives a ferrocene–ferrocenium quasi-reversible process at 0.33 V that is similar to that of a free ppfa ligand ($E_{1/2} = 0.24$ V). Cluster **3** also displays an irreversible reduction at -2.15 V that is assigned to the reduction of the metal core to give the one-electron reduced species $[Os_3(H)(CO)_8(NO_2)(ppfa)]^-$. Since the amine group is a better σ-donor than the phosphine fragment, the coordination of such a good σ-donor in **1** would raise both the HOMO and the LUMO energies by an inductive effect; thus reduction would be more difficult and oxidation becomes easier than in cluster **2**. We therefore assign the one-electron reduction of **2** and **3** as primarily cluster-based and the oxidation as primarily dppf- or ppfa-based. These results show that the cluster and ferrocenyl phosphine moieties are more difficult to reduce and oxidise, respectively, than in the parent cluster **1** and free dppf and ppfa. It is suggested that there is a slight interaction between the ferrocene and the cluster cage frontier orbitals. It is likely that the HOMO is solely ferrocene-based, while the LUMO is primarily cage-based with a significant ferrocene admixture which results in its more difficult reduction.

3. Experimental

3.1. General procedures

All reactions and manipulations were carried out under Ar using standard Schlenk techniques, except for the chromatographic separations. Solvents were purified by standard procedures and distilled prior to use. $[Os_3(\mu\text{-}H)(CO)_{10}(\mu\text{-}\eta^2\text{-}NO_2)]$ (**1**) was prepared according to the reported method [1]. All chemicals, unless otherwise stated, were purchased commercially and used as received. Reactions were monitored by IR spectroscopy and analytical thin-layer chromatography (Merck Kieselgel 60 F_{254}) and the products were separated by thin-layer chromatography on plates coated with silica (Merck Kieselgel 60 GF_{254}). Infrared spectra were recorded on a Bio-Rad FTS-7 IR spectrometer, using 0.5 mm CaF_2 solution cells. ^{1}H-NMR spectra were recorded on a Bruker DPX300 NMR spectrometer using CD_2Cl_2 and referenced to $SiMe_4$ ($\delta = 0$), ^{31}P-NMR spectra on a Bruker DPX500 NMR spectrometer using $CDCl_3$ solvent with 85% H_3PO_4 as a reference. Positive ionisation FAB mass spectra were recorded on a Finnigan MAT 95 mass spectrometer, using *m*-nitrobenzyl alcohol or α-thioglycerol as matrix solvents. Microanalyses were performed on thoroughly dried samples by Butterworth Laboratories, UK.

3.2. Reaction of $[Os_3(\mu\text{-}H)(CO)_{10}(\mu\text{-}\eta^2\text{-}NO_2)]$ (1) with dppf

A solution of **1** (50 mg, 0.055 mmol) in 30 cm^3 CH_2Cl_2 was treated with dppf (30.5 mg, 0.055 mmol) and Me_3NO (6 mg, 0.066 mmol) at r.t. for 12 h. The red solution was concentrated under reduced pressure. Separation of the residue by TLC, with CH_2Cl_2–*n*-hexane (1:1, v/v) as eluent, yielded one intense red band (R_f 0.45). It was characterised as cluster $[Os_3(\mu\text{-}H)(CO)_8(\mu\text{-}\eta^2\text{-}NO_2)(\mu\text{-dppf})]$ (**2**) and recrystallised from a CH_2Cl_2 solution by slow evaporation to give red, block crystals (36 mg, 46%). (Anal. Found: C, 36.4; H, 2.2; N, 1.1; P, 4.6. Calc. for $C_{42}H_{29}NO_{10}P_2FeOs_3$ **2**: C, 36.12; H, 2.08; N, 1.00; P, 4.44%).

3.3. Reactions of $[Os_3(\mu\text{-}H)(CO)_{10}(\mu\text{-}\eta^2\text{-}NO_2)]$ 1 with ppfa

Solid of **1** (50 mg, 0.055 mmol) was reacted with ppfa (25 mg, 0.056 mmol) and Me_3NO (6 mg, 0.066 mmol) in 30 cm^3 CH_2Cl_2 at 40 °C for 4 h. The solvent was removed under reduced pressure, the red residue was dissolved in a minimum amount of CH_2Cl_2 and chromatographed on silica. Elution with CH_2Cl_2–*n*-hexane (4:6, v/v) gave a major orange band (R_f 0.35). It was characterised as cluster $[Os_3(\mu\text{-}H)(CO)_8(\mu\text{-}\eta^2\text{-}NO_2)(\mu\text{-ppfa})]$ (**3**). Cluster **3** was recrystallised from a $CHCl_3$–*n*-hexane solution to give red crystals (28 mg, 40%). (Anal. Found: C, 31.6; H, 2.4; N, 1.2; P, 2.4. Calc. for $C_{34}H_{29}N_2O_{10}PFeOs_3$ **3**: C, 31.82; H, 2.26; N, 1.09; P, 2.42%)

3.4. Electrochemical studies

Electrochemical measurements were carried out by using EG&G Princeton Applied Research (PAR) Model 273A potentiostat/galvanostat connected to an interfaced computer employing PAR 270 electrochemical software. Cyclic voltammograms were obtained at r.t. with a gas sealed (Ar) two compartment cell, equipped with a glassy carbon working electrode (Bioanalytical), platinum wire auxiliary (Aldrich) and $Ag\,|\,AgNO_3$ reference (Bioanalytical) electrodes. *n*-Tetrabutylammonium hexafluorophosphate (TBAHFP), 0.1 mol dm^{-3}, in anhydrous deoxygenated MeCN was used as a supporting electrolyte. Ferrocene was added at the end of each experiment as an internal standard [19]. Potential data (vs. $Ag\,|\,AgNO_3$) were checked against the ferrocene $(0/+1)$ couple; under the actual experimental conditions the ferrocene–ferrocenium couple is located at -0.14 V in MeCN.

Table 4
Crystal data and data collection parameters for compounds **2**, **3**

	2·2CH_2Cl_2	**3**
Empirical formula	$C_{44}H_{33}NO_{10}P_2$-Cl_4FeOs_3	$C_{34}H_{29}N_2O_{10}P$-$FeOs_3$
Formula weight	1565.95	1283.03
Crystal system	Monoclinic	Orthorhombic
Space group	$P2_1/n$ ($\#$ 14)	$P2_12_12_1$ ($\#$ 19)
Unit cell dimensions		
a (Å)	16.957(2)	10.072(1)
b (Å)	11.979(1)	15.909(2)
c (Å)	24.687(2)	22.742(2)
α (°)		
β (°)	103.06(2)	
γ (°)		
U (Å^3)	4885.0(9)	3644.1(6)
Z	4	4
D_{calc} (g cm^{-3})	2.129	2.338
μ (Mo–K_α) (cm^{-1})	84.04	109.12
Crystal colour, habit	Red, block	Red, block
Crystal size (mm)	$0.25 \times 0.26 \times 0.33$	$0.19 \times 0.23 \times 0.24$
Unique reflections	6884	3544
Observed reflections [$F > 3\sigma(F)$]	4618	2578
R	0.036	0.052
R'	0.040	0.061
Goodness-of-fit (S)	1.68	1.72

3.5. Crystallography

Crystals suitable for X-ray analyses were glued on glass fibres with epoxy resin or sealed in 0.3 mm glass capillaries. Intensity data were collected at ambient temperatures either on an Enraf–Nonius CAD4 diffractometer (complex **2**) or on a MAR research image plate scanner (complex **3**) equipped with graphite-monochromated Mo–K_α radiation ($\lambda = 0.710\ 73$ Å) using ω–2θ and ω scan types. Details of the intensity data collection and crystal data are given in Table 4. The diffracted intensities were corrected for Lorentz and polarisation effects. The Ψ scan method was employed for semi-empirical absorption corrections for **2** [20], however, an approximation to absorption correction by inter-image scaling was applied for **3**. Scattering factors were taken from Ref. 21a and anomalous dispersion effects [21b] were included in F_c. The structures were solved by direct methods (SIR88 [22] for **2** and SIR92 [23] for **3**) and expanded by Fourier-difference techniques. Atomic coordinates and thermal parameters were refined by full-matrix least-squares analysis on F, with the osmium, iron, phosphorus and chlorine atoms being refined anisotropically. The metal hydride was located by Fourier-difference synthesis based on low angle data and analysis of CO ligands distribution while those of the organic moieties were generated in their ideal positions (C–H 0.95 Å). The absolute configuration of cluster **3** was established by refining the Flack parameter [0.0027(3)]. Calculations were performed on a Silicon-Graphics computer, using the program package TEXSAN [24].

4. Supplementary material

Crystallographic data (excluding structure factors) for the structural analysis have been deposited with the Cambridge Crystallographic Data Centre, CCDC nos. 154816 and 154817 for complexes **2** and **3**. Copies of this information may be obtained free of charge from The Director, CCDC, 12 Union Road, Cambridge CB2 1EZ, UK (Fax: +44-1223-336033; e-mail: deposit@ccdc.cam.ac.uk or www: http://www.ccdc.cam.ac.uk).

Acknowledgements

We gratefully acknowledge financial support from the Hong Kong Research Grants Council and the University of Hong Kong. B.K.-M. Hui acknowledges the receipt of a postgraduate studentship, administered by the University of Hong Kong.

References

[1] B.K.-M. Hui, W.-T. Wong, J. Chem. Soc. Dalton Trans. (1996) 2177.
[2] B.K.-M. Hui, W.-T. Wong, J. Chem. Soc. Dalton Trans. (1998) 447.
[3] B.K.-M. Hui, W.-T. Wong, J. Chem. Soc. Dalton Trans. (1998) 3977.
[4] C. Kollmar, M. Couty, O. Kahn, J. Am. Chem. Soc. 113 (1991) 7994.
[5] J.S. Millarm, A.J. Epstein, Angew. Chem. Int. Ed. Engl. 33 (1994) 385.
[6] R.W. Wagner, P.A. Brown, T.E. Johnson, J.S. Lindsey, J. Chem. Soc. Chem. Commun. (1991) 1463.
[7] E.C. Constable, Angew. Chem. Int. Ed. Engl. 30 (1991) 407.
[8] P.D. Beer, Z. Chen, M.G.B. Drew, A.J. Pilgrim, Inorg. Chim. Acta 225 (1994) 137.
[9] I.R. Butler, Organometallic Chemistry, in: E.W. Abel (Ed.), Specialist Periodic Reports 21, Royal Society of Chemistry, Letchworth, UK, 1992, p. 338.
[10] A. Togni, T. Hayashi (Eds.), Ferrocenes, VCH, Weinheim, 1995.
[11] S.T. Chacon, W.R. Cullen, M.I. Bruce, O.B. Shawkataly, F.W.B. Einstein, R.H. Jones, A.C. Willis, Can. J. Chem. 68 (1990) 2001.
[12] F.G. Torre, F.A. Jalón, A. López-Agenjo, B.R. Manzano, A. Rodríguez, Organometallics 17 (1998) 4634.
[13] A.J. Blake, A. Harrison, B.F.G. Johnson, E.J.L. Mclnnes, S. Parsons, D.S. Shephard, L.J. Yellowlees, Organometallics 14 (1995) 2160.
[14] S. Onaka, T. Moriya, S. Takagi, A. Mizuno, H. Furuta, Bull. Chem. Soc. Jpn. 65 (1992) 1415.
[15] A. Mernyi, C. Kratky, W. Weissensteiner, M. Widhalm, J. Organomet. Chem. 508 (1996) 209.

[16] H. Brunner, W. Zettlmeier, Handbook of Enantioselective Catalysis with Transition Metal Compounds, VCH, Weinheim, 1993.
[17] M. Sawamura, Y. Ito, Chem. Rev. 92 (1992) 857.
[18] W.-Y. Wong, K.-K. Cheung, W.-T. Wong, J. Chem. Soc. Dalton Trans. (1995) 1379.
[19] G. Gritzner, J. Kute, Pure Appl. Chem. 56 (1984) 461.
[20] A.C.T. North, D.C. Phillips, F.S. Mathews, Acta Crystallogr. Sect. A 24 (1968) 351.
[21] (a) D.T. Cromer, J.T. Waber, Table 2.2B, International Tables for X-Ray Crystallography, Kynoch Press, Birmingham, vol. 4, 1974;
(b) D.T. Cromer, J.T. Waber, Table 2.3.1, International Tables for X-Ray Crystallography, Kynoch Press, Birmingham, vol. 4, 1974.
[22] M.C. Burla, M. Camalli, G. Cascarano, C. Giacovazzo, G. Polidori, R. Spagna, D. Viterbo, J. Appl. Crystallogr. 22 (1989) 389.
[23] A. Altomare, M.C. Burla, M. Camalli, M. Cascarano, C. Giacovazzo, A. Guagliardi, G. Polidori, J. Appl. Crystallogr. 25 (1992) 210.
[24] TEXSAN, Crystal Structure Analysis Package, Molecular Structure Corporation, Houston, TX, 1985 and 1992.